THE JOURNAL OF PHYSICAL CHEMISTRY C
A JOURNAL OF THE AMERICAN CHEMICAL SOCIETY

pubs.acs.org/JPCC

Article

Local Silver Site Temperature Critically Reflected Partial and Complete Photooxidation of Ethanol Using Ag−TiO_2 as Revealed by Extended X-ray Absorption Fine Structure Debye−Waller Factor

Daiki Fukuhara, Moses Tuhafeni Joseph, Tarik Loumissi, Chao Zhang, Takaomi Itoi, Hongwei Zhang, and Yasuo Izumi*

Cite This: *J. Phys. Chem. C* 2021, 125, 14689−14701

Read Online

ACCESS | Metrics & More | Article Recommendations | Supporting Information

ABSTRACT: The critical factors in choosing the reaction pathway for photocatalysis are often unclear. In this study, for a typical Ag−TiO_2 photocatalyst, the control factors of partial and complete oxidation of ethanol were investigated using kinetics, UV−visible and emission spectroscopy, and silver K-edge extended X-ray absorption fine structure. Low concentrations of O_2-derived intermediate species that were not detected by curve-fitting analysis could be monitored under the photocatalytic conditions based on the local temperature of Ag sites provided by the Debye−Waller factor and the correlated Debye model. The site temperature monitoring was extended to Ag nanoparticles growing from 0.5 to 3.6 nm under photocatalytic reaction conditions. The Ag site temperature reached 404 K under reductive conditions to dehydrogenate ethanol into acetaldehyde, whereas it was 363−368 K under oxidative conditions owing to O_2-derived species forming CO_2, CH_4, and H_2O to suppress localized surface plasmon resonance. Under UV light, partial ethanol oxidation to acetaldehyde and O_2 activation for complete oxidation to CO_2 and H_2O proceeded over TiO_2. However, under visible light, the C−C bond cleavage to CO_2 and CH_4 and complete oxidation to CO_2 and H_2O combined with the O_2-derived species transferred from the TiO_2 surface proceeded over Ag^0 nanoparticles.

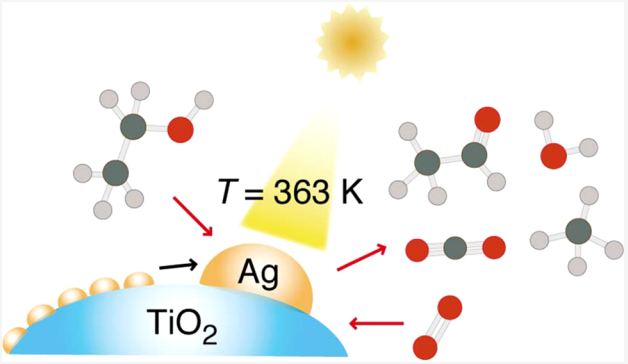

INTRODUCTION

Photocatalysis consists of redox reactions by separated charges, and the photooxidation reaction often proceeds faster than the complementary photoreduction reaction.[1−3] Recently, photoreduction has received much more attention, e.g., the reduction of CO_2 and/or N_2 to fuels/feedstocks.[4,5] Metal oxide/hydroxide semiconductors are used as the major components of photocatalysts because they are often inexpensive and easy to handle, e.g., TiO_2.[6] Among them, it remains open for discussion how to control partial[7] and complete photooxidation reactions that are key techniques for sustainable applications.[1]

In this paper, the most typical photocatalyst consisting of metal oxide (TiO_2) and metal nanoparticles (Ag) is chosen, and the processes of photocatalytic dehydrogenation (partial oxidation) and complete oxidation to CO_2 and H_2O were tested. The key reaction mechanism to select each product was investigated by extended X-ray absorption fine structure (EXAFS), based on the Fourier transform, curve-fit analysis, and the interpretation of the Debye−Waller factor.[8,9]

Although the trapping effect of excited electrons on metal nanoparticles transferred from the conduction band (CB) of a metal oxide semiconductor has been widely accepted,[10−12] excited electrons owing to localized surface plasmon resonance (LSPR) transferring to metal oxides[13,14] and/or adsorbed molecules[12] have also been reported. Recently, the origins of the photocatalytic reaction steps have been investigated: consecutive reaction mechanism (1) to reduce CO_2 to CO on ZrO_2 owing to charge separation at the band gap (BG) and (2) subsequent H_2 and/or H_2O activation over the Ag/Au nanoparticle surface owing to heat converted from LSPR spilling over reactive H species to the CO_2 reduction sites over ZrO_2.[15,16] Using Ni nanoparticles, the subsequent reaction (2′) consisted of further reduction steps of CO to methane (CH_4) owing to heat converted from absorbed light energy.[17]

The photooxidation rates of ethanol were on the order of >1 mmol h^{-1} g_{cat}^{-1} in comparison to CO_2 photoreduction rates under reductive conditions: <1 mmol h^{-1} g_{cat}^{-1}.[15−17] The oxidation states of active Ag sites and the reactive oxygen species

Received: May 7, 2021
Revised: June 18, 2021
Published: July 1, 2021

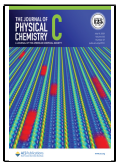

https://doi.org/10.1021/acs.jpcc.1c04076
J. Phys. Chem. C 2021, 125, 14689−14701

were monitored simultaneously by the peak intensities of Ag−O and Ag−Ag interatomic pairs in the Fourier transform and the Debye−Waller factor of EXAFS. The local temperature monitoring via the Debye−Waller factor based on the correlated Debye model[8,9] was advantageous to monitor atomic-level local catalytically active elements.

Among the atomic-level state-of-the-art techniques, EXAFS directly monitors the thermal vibration of X-ray-absorbing atoms in contrast to surface-enhanced Raman scattering (SERS) monitoring which requires a probe molecule, e.g., *p*,*p*′-dimercaptoazobenzene[18,19] or adonitol,[20] phonon monitoring by Raman which requires Si dots in the Au cavity,[21] Raman spectroscopy which requires locally doped ions, e.g., Yb^{3+} and Er^{3+},[22] and absorption spectroscopy for Au nanoparticles which requires laser irradiation.[23] The local temperature monitoring by EXAFS has been reported for Ag, Au, and Ni nanoparticles over ZrO_2 under CO_2, H_2 (or H_2O), and UV−visible light, but the temperature increase exclusively originated from light energy because of the slow reaction rates to convert thermodynamically stable CO_2.[15−17] In this paper, the exothermic heats of partial (eq 1) and complete (eq 2) oxidation reactions of ethanol were monitored as well as the heat converted from irradiated UV−visible light.

$$C_2H_5OH + 1/2O_2 \rightarrow CH_3CHO + H_2O$$
$$\Delta_r H^\circ = -172.91 \text{ kJ mol}^{-1} \quad (1)$$

$$C_2H_5OH + 3O_2 \rightarrow 2CO_2 + 3H_2O$$
$$\Delta_r H^\circ = -1277.38 \text{ kJ mol}^{-1} \quad (2)$$

EXPERIMENTAL SECTION

Catalyst Preparation. $AgNO_3$ (0.160 g; purity >99.8%, Wako Pure Chemical, Japan) and TiO_2 (3.30 g; P25 Evonik, Essen, Germany, specific surface area 60 $m^2\ g^{-1}$ and anatase:rutile phase = 8:2) were mixed in pure water (50 mL, <0.055 $\mu S\ cm^{-1}$), agitated by ultrasound (430 W, 38 kHz) for 10 min, and stirred at 353 K and 850 rotations/min for 1 h.[24,25] The obtained white precipitate was filtered using a poly(tetrafluoroethylene)-based membrane filter (Omnipore JVWP04700, Millipore, Burlington, MA; pore size 0.1 μm) and washed using pure water (each 50 mL) five times. Then, the product was dried at 373 K for 24 h, followed by heating to 673 K at a ramping rate of 9.9 K min^{-1}, and maintained at 673 K for 2 h. The obtained light yellow powder became gray overnight because of the oxidation of Ag^0 formed by heating to Ag^I_2O, which is a stable state at 293 K. The Ag content in the sample was determined to be 2.0 wt % based on X-ray absorption edge jump (see the X-ray Absorption Fine Structure (XAFS) Measurements section below). The final product was denoted as Ag (2.0 wt %)−TiO_2.

Photocatalytic Oxidation Tests. The photooxidation tests of ethanol were performed in a closed circulation system (total inner volume 202.7 mL including the reactor and two sampling sections) connected to a vacuum using rotary and diffusion pumps (10^{-6} Pa). The photocatalyst samples (0.100 g) were homogeneously dispersed in a flat-cylinder quartz reactor (bottom area 23.8 cm^2; inner volume 48.8 mL),[26,27] connected to the closed circulation system and evacuated for 2 h. Then, ethanol (1.33 kPa) and/or O_2 (2.67 or 5.32 kPa) was introduced into the quartz reactor. The molar amount of ethanol was 6.0 times that of Ag atoms in the sample. The amount was suppressed from saturated pressure (4.91 kPa @290 K) to monitor consecutive reaction to acetaldehyde and then to CO_2 and H_2O (eqs 1 and 3).

$$CH_3CHO + 5/2O_2 \rightarrow 2CO_2 + 2H_2O$$
$$\Delta_r H^\circ = -1104.47 \text{ kJ mol}^{-1} \quad (3)$$

As the partial dehydration (eq 1) and complete oxidation of ethanol (eq 2) require 0.5 and 3 equiv of O_2, we varied the C_2H_5OH:O_2 ratio between 1:0 and 1:4 to obtain insight into the reaction mechanism.

The photocatalyst was irradiated with UV−visible light from a 500 W xenon arc lamp (Ushio, Tokyo, Japan; model UI-502Q) from the bottom of the quartz cell for 5 h. The distance between the light exit and the photocatalyst sample was 10 mm. The light intensity was 70 mW cm^{-2} at the center of the photocatalyst position.[28] In-profile kinetic data were collected as a function of the light's excitation wavelength by inserting a sharp-cut filter at each fiber light exit. L39 and U330 (2.5 mm thick; Hoya, Japan) filters were used to pass light with wavelengths of >390 nm (L39), 245 < λ < 386 nm, and >686 nm (U330).[29] A control kinetic test irradiated by UV−visible light while the Ag (2.0 wt %)−TiO_2 photocatalyst and the reactor were immersed in a quartz bath filled with water controlled at 295 K was also performed.

The gas composition during the light irradiation was monitored using an online gas chromatograph equipped with a thermal conductivity detector (Shimadzu, Kyoto, Japan; Model GC-8AT). A packed column of Molecular Sieves 13X-S (3 m length, 3 mm internal diameter; GL Sciences Inc., Japan) was used for the separation of O_2, N_2, CH_4, and CO, and a packed column of poly(ethylene glycol)-6000/Flusin P (3 m length, 3 mm internal diameter, GL Sciences) was also used for the separation of CO_2, CH_3CHO, acetone, C_2H_5OH, and H_2O. Helium (0.13 MPa, purity >99.9999%) was used as the carrier gas. However, argon (0.13 MPa, purity >99.998%) was used as the carrier gas for the separation of H_2 through the packed column of Molecular Sieves 13X-S.

UV−Visible Spectroscopy. UV−visible spectra were recorded on a double-beam model V-650 spectrophotometer using D_2 and halogen lamps below and above 340 nm, respectively, equipped with a photomultiplier tube and an integrated ISV-469 sphere (JASCO, Tokyo, Japan) for diffuse-reflectance detection. The wavelength range was 200−800 nm. The data were transformed using the Kubelka−Munk function. Fresh photocatalyst samples and those used in various photocatalytic reaction conditions were quickly set in a sample holder for UV−visible spectrum measurements. A poly(tetrafluoroethylene) plate was used as the reference.

Fluorescence Spectroscopy. The absorption−fluorescence spectra were recorded on an FP-8600 (JASCO; Chiba Iodine Resource Innovation Center) using a 150 W Xe arc lamp (UXL-159, Ushio) equipped with a photomultiplier tube. The excitation was at 300−480 nm, and the fluorescence range was 350−800 nm. The incident excitation light from the Xe lamp was monitored using a Si photodiode, and the monitored fluorescence light emitted from the sample was normalized on the basis of the incident light intensity at each wavelength. The photocatalyst powder (2.0 mg) was mixed with purified water (3.0 mL) and ultrasonicated (430 W, 38 kHz) for 30 min. All spectra were recorded for the suspensions in a quartz cell at 295 K.

https://doi.org/10.1021/acs.jpcc.1c04076
J. Phys. Chem. C 2021, 125, 14689−14701

Transmission Electron Microscopy (TEM) Measurements. TEM was performed using a JEM-2100F (JEOL) equipped with a field-emission gun (acceleration voltage of 200 kV) at the Center for Analytical Instrumentation. The samples were mounted on a Cu mesh (250 meshes per inch) coated with carbon and a copolymer film of poly(vinyl alcohol) and formaldehyde (Formvar, Monsanto, St. Louis, MO).

X-ray Absorption Fine Structure (XAFS) Measurements. Silver K-edge XAFS spectra were measured at 290 K in transmission mode at the Photon Factory Advanced Ring, High Energy Accelerator Research Organization (KEK, Tsukuba, Japan), on the NW10A beamline. A Si (311) double-crystal monochromator and a Pt-coated focusing cylindrical mirror were inserted in the path of the X-ray beam. A piezotransducer was used to detune the X-rays to two-thirds of the maximum intensity to suppress higher harmonics. The Ag K-edge absorption energy was calibrated at 25 516.5 eV using the X-ray spectrum of a Ag metal foil (40 μm thick).[30]

A disk (Φ = 10 mm) of a Ag (2.0 wt %)−TiO_2 photocatalyst (140 mg) was set in a Pyrex glass reactor equipped with a Kapton film (Dupont, Wilmington, DE; 50 μm thick) for X-ray transmission and a poly(ethylene terephthalate) (PET) film (Toyobo Film Solutions, Japan, G2; 38 μm thick) for both UV−visible light and X-ray transmission filled with 1.33 kPa of ethanol and 2.67 or 5.32 kPa of O_2. The sample was irradiated with UV−visible light from a Xe arc lamp through the PET film at the beamline (Figure S1, Supporting Information).[15−17] As control tests, Ag K-edge XAFS spectra were measured for the Ag (2.0 wt %)−TiO_2 photocatalyst (140 mg) under 1.33 kPa of ethanol and 2.67 kPa of O_2 irradiated with light from a Xe arc lamp filtered by L39 and U330 filters to confirm the light wavelength dependence and under 1.33 kPa of ethanol at 301−403 K using an electric furnace at the beamline to confirm the temperature evaluated on the basis of the correlated Debye model.[8,9]

The obtained Ag K-edge XAFS data were analyzed using the XDAP software package.[31] The pre-edge background was approximated with a modified Victoreen function, i.e., $C_2/E^2 + C_1/E + C_0$, where E is the photon energy. The background for postedge oscillation, μx, was approximated with a smoothing spline function and was calculated for a particular number of data points:

$$\sum_{i=1}^{\text{data points}} \frac{(\mu x_i - \text{background}_i)^2}{\exp(-0.075k_i^2)} \leq \text{smoothing factor} \quad (4)$$

where k is the angular photoelectron wavenumber.

Multiple-shell curve-fit analyses were performed on the Fourier-filtered k^3-weighted EXAFS data in k- and R-space (R: interatomic distance) based on the plane-wave approximation for amplitude $A_i(k)$, coordination number N_i, backscattering amplitude $f_i(k)$, Debye−Waller factor σ_i, and mean free photoelectron path λ for shell i:

$$A_i(k) = \frac{N_i}{kR_i^2}|f_i(k)| \exp\left[-2\left(\sigma_i^2 k^2 + \frac{R_i}{\lambda}\right)\right], \; i = \text{Ag, O} \quad (5)$$

using the empirical amplitude extracted from the EXAFS data for the Ag metal foil (40 μm thick) and Ag_2O powder. The R values for the Ag−Ag and Ag−O interatomic pairs were set to 0.2889 nm with the N value of 12[32] and 0.2044 nm with the N value of 2, respectively.[33] We assumed that the many-body reduction factor, S_0^2, is identical for both the sample and the reference.

RESULTS AND DISCUSSION

Photocatalytic Oxidation Tests. The photocatalytic oxidation tests of ethanol using TiO_2 and Ag (2.0 wt %)−TiO_2 catalysts are summarized in Figures 1 and 2. CO was not detected above the detection limit (0.2 nmol) while the maximum H_2 evolved was 0.79 μmol in 5 h of reaction, and the amount was negligible throughout this study. Furthermore, the authors could not distinguish between the ethanol adsorption (Scheme 1A-b and B-b) and carbonaceous deposition.

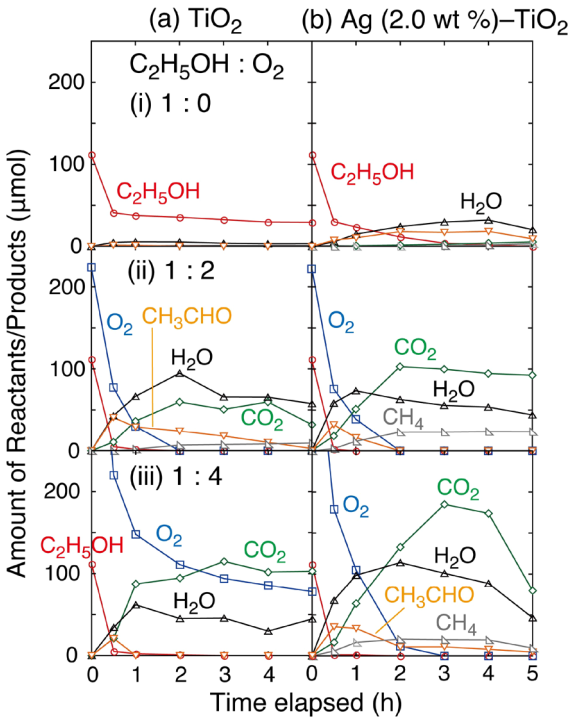

Figure 1. Time course changes in the photocatalytic tests during exposure to (i) C_2H_5OH (1.33 kPa), (ii) C_2H_5OH (1.33 kPa) and O_2 (2.67 kPa), and (iii) C_2H_5OH (1.33 kPa) and O_2 (5.32 kPa) using (a) TiO_2 and (b) Ag (2.0 wt %)−P25 irradiated by UV−visible light. The amount of photocatalyst was 0.100 g.

The time course of ethanol photooxidation under various conditions using TiO_2 and Ag (2.0 wt %)−TiO_2 is summarized in Figure 1. Using TiO_2 (0.100 g), C_2H_5OH (1.33 kPa), and UV−visible light, any reactions proceeded negligibly (Figure 1a-i). Of the introduced ethanol (112 μmol), 29.3 μmol remained in the gas phase at 5 h of reaction. Therefore, 73.8% adsorbed as ethoxy and hydroxy species over the TiO_2 surface (Scheme 1A-a and b) before 5 h of reaction, similar to a recent report.[34]

Using TiO_2 (0.100 g), C_2H_5OH (1.33 kPa), O_2 (2.67 kPa), and UV−visible light (Figure 1a-ii), the initial formation rates of CH_3CHO and H_2O were 816 and 860 μmol h^{-1} g_{cat}^{-1}, respectively, following eq 1 for 30 min of reaction. Then, CO_2 was consecutively formed from CH_3CHO at the rate of 512 μmol h^{-1} g_{cat}^{-1} via eq 3 between 30 min and 2 h of reaction.

Similar consecutive photooxidation of C_2H_5OH to CH_3CHO and then CO_2 was reported using Ag−TiO_2−montmorillonite under ethanol and moisture.[35] Thus, the TiO_2 surface activated O_2 (Scheme 1B-c) as reported in the literature.[7] The molar

https://doi.org/10.1021/acs.jpcc.1c04076
J. Phys. Chem. C 2021, 125, 14689−14701

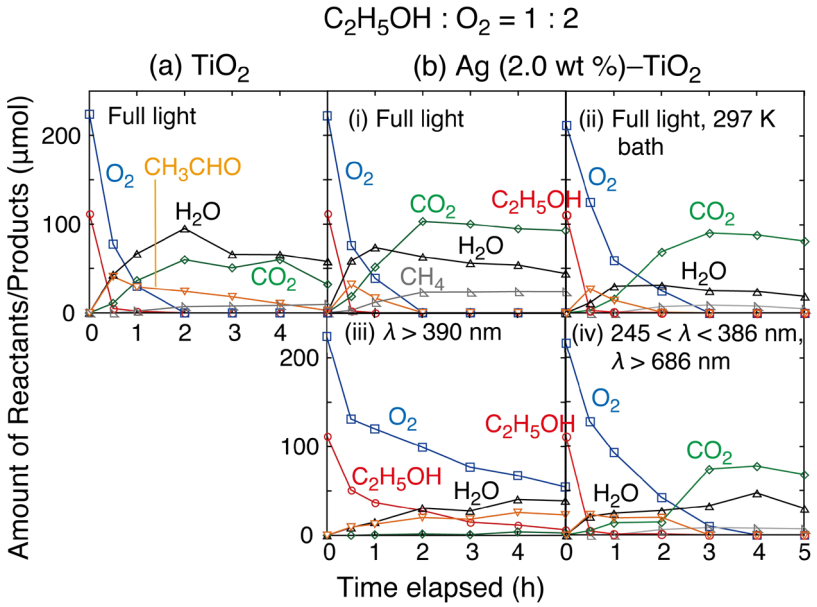

Figure 2. Time course changes in the photocatalytic tests during exposure to C_2H_5OH (1.33 kPa) and O_2 (2.67 kPa) using (a) TiO_2 irradiated under full light and (b) Ag (2.0 wt %)−TiO_2 irradiated under (i) full light, (ii) full light and at 297 K, (iii) visible light of $\lambda > 390$ nm, and (iv) UV and IR light of $245 < \lambda < 386$ nm and $\lambda > 686$ nm. The amount of photocatalyst was 0.100 g.

Scheme 1. Major Reaction Steps that Occurred Using (A) Ag−TiO_2 Photocatalyst, Ethanol, and UV−Visible Light Irradiation and (B) Ag−TiO_2 Photocatalyst, Ethanol, O_2, and UV−Visible Light Irradiation

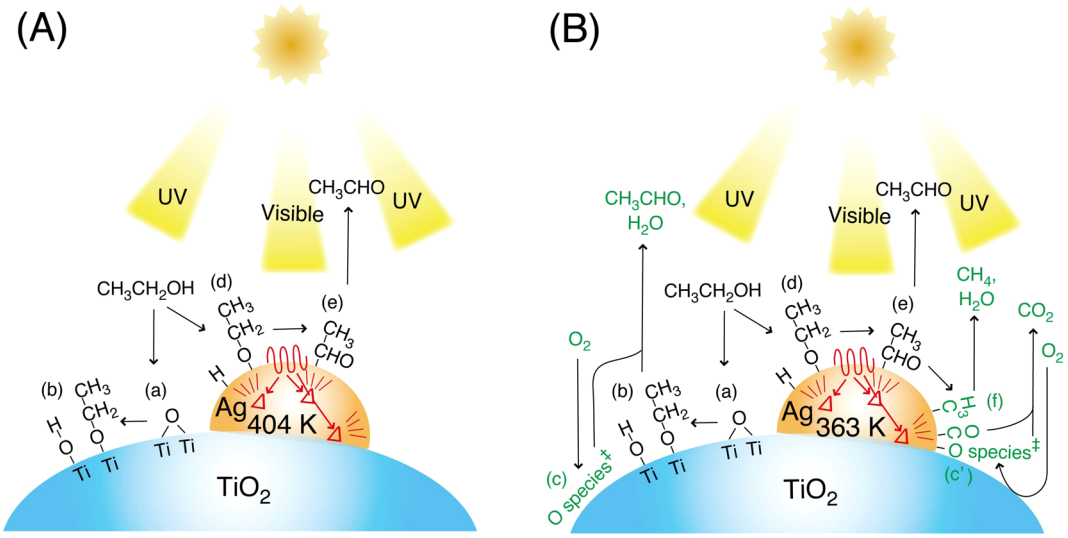

amount of formed H_2O during the period was equal to that of CO_2, exactly following the stoichiometry of eq 3.

When the initial molar ratio of ethanol:O_2 changed from 1:2 to 1:4 (Figure 1a-iii), complete oxidation reaction via eq 2 became predominant, and the amount of CO_2 produced (115 μmol) was 1.92 times greater than that under ethanol:O_2 of 1:2 (Figure 1a-ii). However, the amount was still 51.4% of that expected if eq 2 completely proceeded. Furthermore, H_2O formation (61.8 μmol) stopped after more than 1 h of reaction (Figure 1a-iii), implying incomplete oxidation reaction including TiO_2 surface species, e.g.,

$$C_2H_5OH + 7/4O_2 \rightarrow CO_2 + 1/2H_2O + CH_3(\text{surface}) + 2HO(\text{surface}) \quad (6)$$

Next, the Ag (2.0 wt %)−TiO_2 photocatalyst was tested. Under C_2H_5OH gas only, CH_3CHO was formed slowly: 18.4 μmol over Ag nanoparticles until 4 h of reaction (Figure 1b-i and Scheme 1A-d and e). The molar amount was half of the Ag atoms (27.8 μmol) contained in the photocatalyst (0.100 g), indicating the following noncatalytic reaction reducing Ag^I sites.

$$C_2H_5OH + Ag_2O \rightarrow CH_3CHO + H_2O + 2Ag \quad \Delta_r H^\circ = -141.86\ \text{kJ mol}^{-1} \quad (7)$$

Essentially equivalent ethanol photodecomposition rates were reported using Ag−TiO_2, Ag_2O−TiO_2, and AgO−TiO_2 photocatalysts irradiated with a low-pressure Hg lamp,[36] suggesting that the Ag sites in all these catalysts were reduced to the Ag^0 state under ethanol and UV light. This noncatalytic reaction proceeded significantly more slowly (18.4 μmol h^{-1} g_{cat}^{-1}) than

https://doi.org/10.1021/acs.jpcc.1c04076
J. Phys. Chem. C 2021, 125, 14689−14701

the photocatalytic reaction using O_2 over TiO_2 (816 μmol h^{-1} g_{cat}^{-1}, Figure 1a-ii). The H_2O formation was 74% greater than the CH_3CHO formation contradicting the stoichiometry of eq 7. The extra water was due to the dehydration of ethanol. If the contribution of the noncatalytic reaction (eq 7) is excluded, the photocatalytic activity of ethanol decomposition using TiO_2 and Ag−TiO_2 was essentially zero in the absence of O_2. There was only 20% increase in the ethanol photodecomposition rate using TiO_2 and Ag−TiO_2 in the presence of moisture irradiated by light-emitting diode light (λ = 405 nm).[37]

When C_2H_5OH (1.33 kPa) and O_2 (2.67 kPa) were introduced, CH_3CHO, H_2O, and CO_2 were formed at a molar ratio of 1:1.82:0.57 until 30 min of reaction (Figure 1b-ii), which was different from the ratio of 1:1.05:0.26 using TiO_2 (Figure 1a-ii), suggesting that both partial oxidation to CH_3CHO via eq 1 over TiO_2 and complete oxidation to CO_2 via eq 2 over Ag nanoparticles occurred. The products between 30 min and 2 h of reaction were CO_2 and CH_4, whereas CH_3CHO was completely consumed until 2 h of reaction. Thus, complete oxidation via eqs 1 and 3 and dissociative redox reaction via eq 8 proceeded over the Ag nanoparticles (Scheme 1B-d−f) in contrast to the slower consecutive reactions of eqs 1 (Scheme 1B-a−c) and 3 over TiO_2.

$$C_2H_5OH + O_2 \rightarrow CO_2 + CH_4 + H_2O$$
$$\Delta_r H^\circ = -475.04 \text{ kJ mol}^{-1} \quad (8)$$

When the initial molar ratio of ethanol:O_2 was changed from 1:2 to 1:4 (Figure 1b-iii), complete oxidation reaction over Ag nanoparticles became predominant because sufficient O_2 was supplied for the reaction of eq 2 (ethanol:O_2 = 1:3). Total C-containing products (185 μmol of CO_2, 20.5 μmol of CH_4; in total 206 μmol) accounted for the complete conversion of ethanol into products by the effects of Ag, while a part of the hydroxy/water remained on the photocatalyst surface based on the formed water (114 μmol, 1.38 kPa). The formed water was still less than the water-saturated pressure (2.6 kPa).

A control experiment was performed to evaluate the effect of catalyst heating converted from irradiated light energy.[15−17] When the catalyst was irradiated using UV−visible light while keeping the reactor at 297 K using a water bath, CH_4 was negligibly formed (Figure 2b-ii). In contrast, consecutive oxidation of C_2H_5OH to CH_3CHO (eq 1) and then to CO_2 (eq 3) proceeded similar to the test under UV−visible light (Figure 2b-i). The reaction of eq 8 negligibly proceeded while C_2H_5OH was consecutively oxidized to CO_2 and H_2O over TiO_2 and Ag nanoparticles (Scheme 1B-a−e) at 297 K. In fact, the formed CO_2 was equal to that in Figure 2b-i if the amount of CH_4 was subtracted on the basis of the stoichiometry of eq 8. The amount of water formed was half that in Figure 2a, implying water adsorption over Ag nanoparticles at 297 K.

Next, the fast major complete oxidation reaction using C_2H_5OH (1.33 kPa), O_2 (2.67 kPa), and Ag (2.0 wt %)−TiO_2 irradiated under UV−visible light was compared with that under visible light, λ > 390 nm (Figure 2b-iii). Complete oxidation and/or dissociative redox reactions were suppressed almost completely, whereas 25.7 μmol of CH_3CHO and 40.5 μmol of H_2O were formed until 4 h of reaction similar to the time course irradiated under UV−visible light but in the absence of O_2 (Figure 1b-i). Thus, dehydrogenation of ethanol (eqs 1 and 7; Scheme 1B-d and e) effectively proceeded over the Ag nanoparticles owing to the heat (see the EXAFS section below) transformed from LSPR by the visible light irradiation. The excited O species on TiO_2 irradiated by UV light resulting in charge separation at the BG was found to be indispensable for the formation of CO_2 and CH_4 (Scheme 1B-c′ and f).

Conversely, using a filter to pass light of 245 < λ < 386 nm and λ > 686 nm to pass UV and IR light, the time course (Figure 2b-iv) resembled that irradiated under UV−visible light at 297 K (Figure 2b-ii). Thus, heated Ag nanoparticles converted from light energy proceeded along the dissociative redox reaction via eq 8, and the origin of the energy should be from visible light. The reaction of eq 3 proceeded much more slowly over Ag nanoparticles at 297 K than that at 363−368 K owing to light irradiation; however, the reaction of eq 3 proceeded well after 2 h of reaction (Figure 2b-iv) due to a self-acceleration mechanism by exothermic heat (see the EXAFS section).

UV−Visible Spectra. The absorption edge of the spectrum for fresh TiO_2 was extrapolated to 369.6 nm (Figure 3a),

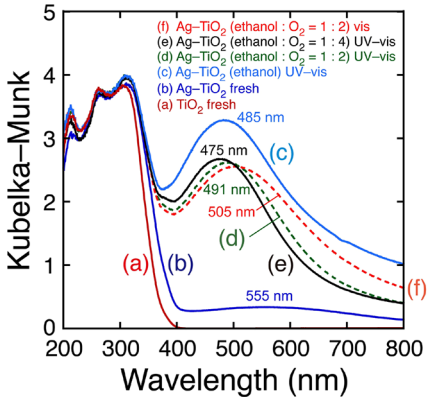

Figure 3. UV−visible spectra for (a) TiO_2 and (b−f) Ag (2.0 wt %)−TiO_2 photocatalysts as (a, b) fresh and after photocatalytic tests under (c) C_2H_5OH (1.33 kPa), (d, f) C_2H_5OH (1.33 kPa) and O_2 (2.67 kPa), and (e) C_2H_5OH (1.33 kPa) and O_2 (5.32 kPa) irradiated by (c−e) UV−visible light and (f) visible light (λ > 390 nm).

corresponding to the BG of 3.3 eV for the anatase phase. In the spectrum for fresh Ag (2.0 wt %)−TiO_2, the absorption edge appeared to shift upward because of the very broad absorption in the whole wavelength range by Ag_2O nanoparticles.

All the spectra for Ag (2.0 wt %)−TiO_2 photocatalysts used for ethanol photooxidation reactions irradiated under UV and/or visible light exhibited a typical intense peak at 475−505 nm (Table 1), demonstrating that the Ag sites were reduced under ethanol to the Ag^0 state and exhibited LSPR when irradiated by visible light. The peak maximum shifted toward a lower wavelength as the Ag nanoparticle size became smaller because of the quantum size effect except for one irradiated under visible light[38] (Table 1) as discussed in the EXAFS section.

Fluorescence Spectra. When the excitation was at 300 nm for the TiO_2 sample, corresponding to greater energy than that of the BG excitation, major peaks due to the band-edge emission appeared at 399 and 417 nm (Figure 4). By the addition of Ag species [Ag_2O for fresh Ag (2.0 wt %)−TiO_2 sample], the peak intensities of major peaks as well as minor peaks at 452, 470, and 573 nm related to interband levels[39] were effectively suppressed owing to charge separation between TiO_2 and Ag_2O particles. A new peak appearing at 376 nm for the Ag (2.0 wt %)−TiO_2 photocatalyst used under C_2H_5OH and O_2 (ratio 1:2) and UV−visible light would be associated with the excitation at the TiO_2 BG combined with LSPR excitation[40] and/or the band-edge emission due to more unsaturated TiO_2.[39]

https://doi.org/10.1021/acs.jpcc.1c04076
J. Phys. Chem. C 2021, 125, 14689−14701

Table 1. Coordination Number (N) of the Ag−Ag Interatomic Pair, Evaluated Ag Nanoparticle Size ($\bar{d}$) and Dispersion (D) Based on EXAFS for Ag (2.0 wt %)−TiO_2, and Absorption Peak Maximum in UV−Visible Spectroscopy

	gas (kPa)			before light irradiation			10 or 20 min of light irradiation			converged @ >160 min light and light off			
entry	ethanol	O_2	light	N^a	$\bar{d}$ (nm)^b	D^c	N^a	$\bar{d}$ (nm)^b	D^c	N^a	$\bar{d}$ (nm)^b	D^c	abs. peak max (nm)
i	1.33	0	full light	3.2	0.65	1.0	8.3	1.9	0.64	10.1	3.6	0.38	485
ii		2.67		3.2	0.65	1.0	5.9	1.1	0.89	9.6	3.1	0.45	491
iii		5.32		2.5	0.50	1.0	5.5	1.1	0.93	8.6	2.1	0.60	475
ii′		2.67	λ > 390 nm	3.2	0.65	1.0	6.6	1.2	0.82	8.7	2.2	0.59	505
ii″			245 nm < λ < 386 nm, λ > 686 nm	4.0	0.80	1.0	5.4	1.0	0.94	8.1	1.8	0.66	

^{a}Obtained based on EXAFS. $^b\bar{d}$ values estimated based on the N value and ref 46. ^cD values estimated based on the N value and ref 46.

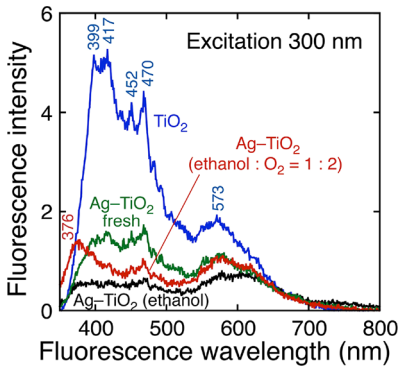

Figure 4. Fluorescence spectra for TiO_2 and Ag (2.0 wt %)−TiO_2 photocatalysts as fresh and after photocatalytic tests under (i) C_2H_5OH (1.33 kPa) and (ii) C_2H_5OH (1.33 kPa) and O_2 (2.67 kPa). The excitation wavelength was 300 nm.

The fluorescence level became the lowest for the Ag (2.0 wt %)−TiO_2 photocatalyst used under ethanol and UV−visible light. The effective charge transfer from TiO_2 CB to metallic Ag nanoparticles should be the reason as shown in the most intense LSPR absorption peak at 485 nm under these conditions (Figure 3c) and O-free metallic Ag surface in comparison to Ag nanoparticles under C_2H_5OH, O_2, and UV−visible light (Figure 3d) on which O_2-derived species adsorbed (see the following EXAFS section).

TEM Images. The changes of the Ag (2.0 wt %)−TiO_2 sample were observed by TEM. For the sample calcined at 673 K for 2 h, nanocrystals of TiO_2 (10−50 nm) were observed (Figure 5a). In the HR-TEM image (Figure 5a, bottom), lattice fringes of anatase TiO_2(101) were observed with the intervals of 0.349 nm (theoretical 0.3517 nm[41]), and those of rutile TiO_2 (200) were also observed with the intervals of 0.230 and 0.223 nm (theoretical 0.22969 nm[41]). When the sample was under C_2H_5OH (1.33 kPa), O_2 (2.67 kPa), and UV−visible light for 20 min, nanocrystals of TiO_2 and the lattice fringes with the intervals of 0.349, 0.341, and 0.346 nm were observed due to the anatase TiO_2(101) lattice (Figure 5b). In contrast, no images for the Ag cluster/nanoparticle were observed.

For the sample under C_2H_5OH (1.33 kPa), O_2 (2.67 kPa), and UV−visible light for 5 h, the Ag(111) lattice was observed with the intervals of 0.229 nm (theoretical 0.2359 nm[32]) as well as the anatase TiO_2(101) lattice with the intervals of 0.349 nm (Figure 5c). The Ag nanoparticles were detected in the TEM image as indicated by arrows (Figure 5c, top).

EXAFS Monitoring. The Fourier transforms of the EXAFS spectra monitoring for Ag (2.0 wt %)−TiO_2 under various photocatalytic reaction conditions (Figures 1b and 2b) are summarized in Figure 6. Its associated k^3-weighted EXAFS χ-

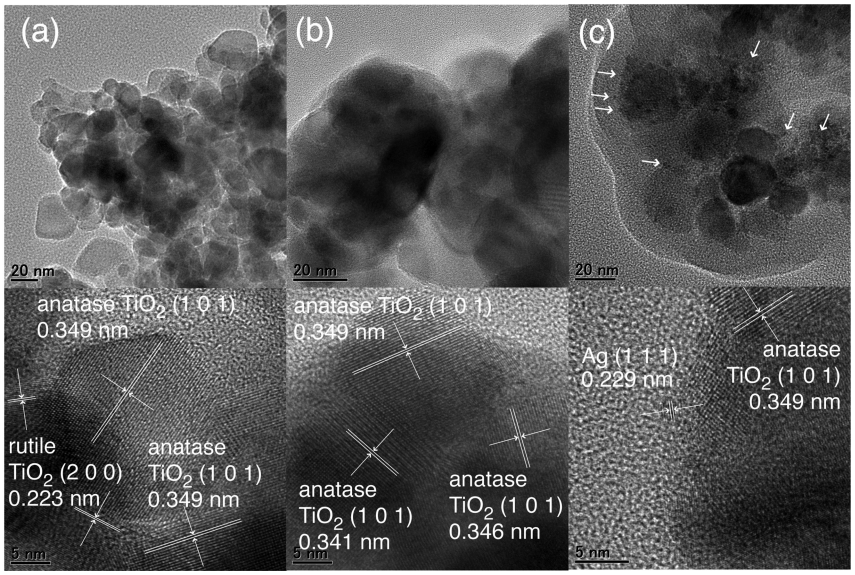

Figure 5. TEM (top column) and high-resolution TEM (bottom column) images observed for Ag (2.0 wt %)−TiO_2 samples (a) calcined at 673 K for 2 h and (b, c) sample (a) under C_2H_5OH (1.33 kPa), O_2 (2.67 kPa), and UV−visible light for 20 min (b) and 5 h (c). The arrows in the TEM image indicate Ag nanoparticles.

https://doi.org/10.1021/acs.jpcc.1c04076
J. Phys. Chem. C 2021, 125, 14689−14701

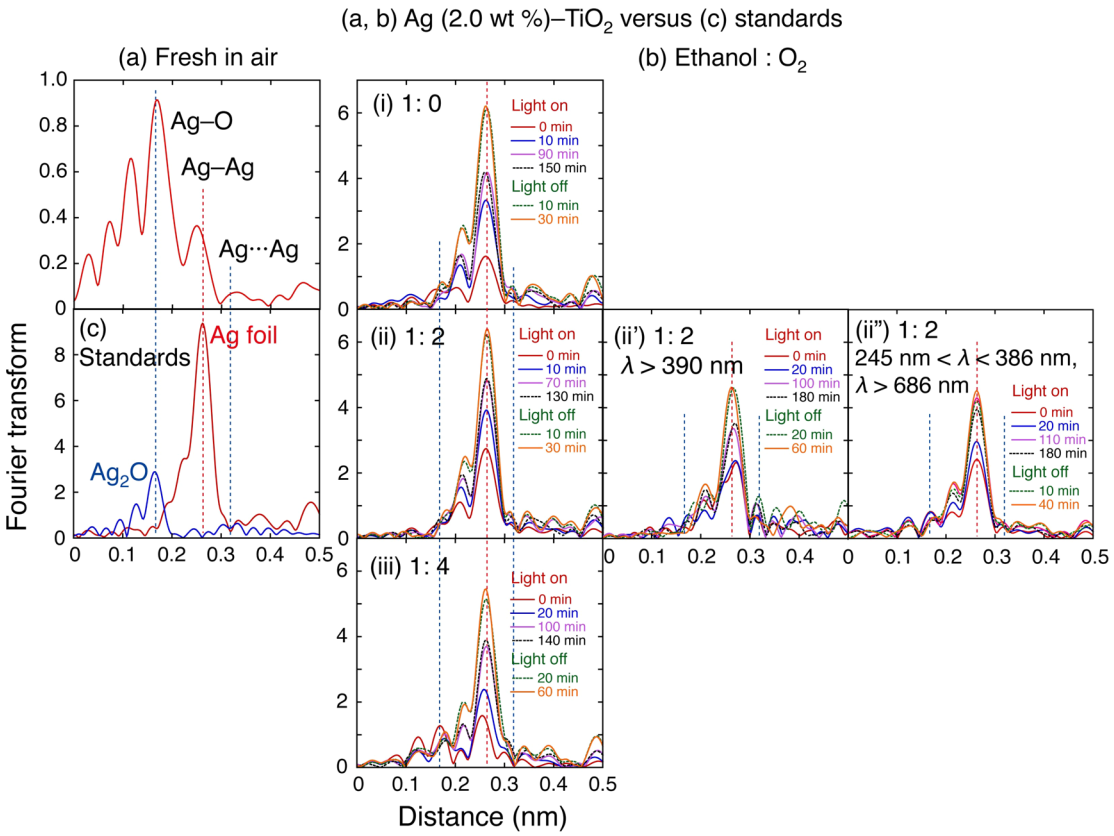

Figure 6. Time course changes of the Fourier transform obtained from the k^3-weighted Ag K-edge EXAFS χ-function for Ag (2.0 wt %)−TiO_2 (a) fresh in air and (b) under C_2H_5OH (1.33 kPa) irradiated by UV−visible light (i), C_2H_5OH (1.33 kPa) and O_2 (2.67 kPa) by UV−visible light (ii), C_2H_5OH (1.33 kPa) and O_2 (2.67 kPa) by visible light ($\lambda > 390$ nm) (ii′), C_2H_5OH (1.33 kPa) and O_2 (2.67 kPa) by UV and IR light (245 nm < λ < 386 nm, $\lambda >$ 686 nm) (ii″), and C_2H_5OH (1.33 kPa) and O_2 (5.32 kPa) by UV−visible light (iii) followed by dark conditions ((i), (ii), (ii′), (iii), and (c): reference spectra for Ag metal foil and Ag_2O powder).

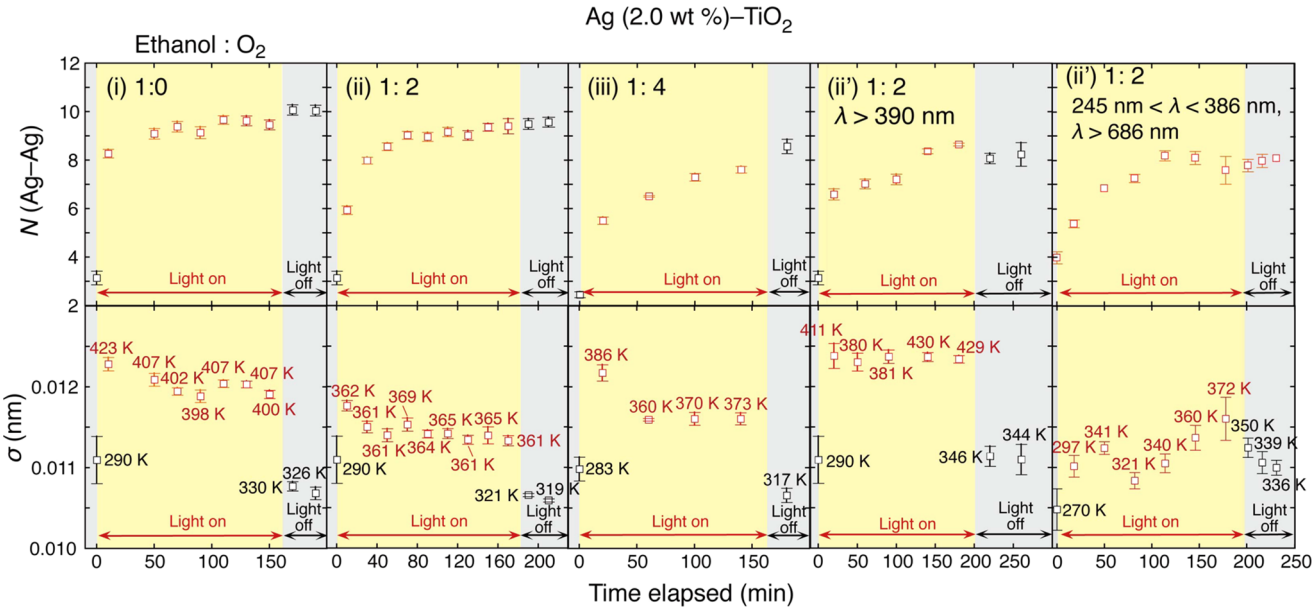

Figure 7. Time course of the coordination number (N, top) and the Debye−Waller factor (σ, bottom) of the Ag−Ag interatomic pair in the EXAFS measured for Ag (2.0 wt %)−TiO_2 using (i) C_2H_5OH and UV−visible light, (ii) C_2H_5OH and O_2 with the molar ratio of 1:2 and UV−visible light, (iii) C_2H_5OH and O_2 with the molar ratio of 1:4 and UV−visible light, (ii′) C_2H_5OH and O_2 with the molar ratio of 1:2 and visible light ($\lambda > 390$ nm), and (ii″) C_2H_5OH and O_2 with the molar ratio of 1:2 and UV and IR light (245 nm < λ < 386 nm, $\lambda >$ 686 nm).

functions are also listed in Figure S2. The Ag (2.0 wt %)−TiO_2 sample prepared just after heating at 673 K was light yellow, demonstrating the presence of the Ag^0 state, whereas the color turned to gray under air overnight, indicating oxidation to

https://doi.org/10.1021/acs.jpcc.1c04076
J. Phys. Chem. C 2021, 125, 14689−14701

$Ag^{I}_{2}O$.[25] The Ag_2O formation was confirmed in the Fourier transform for the sample in air overnight (Figure 6a) compared with the data for the standard Ag_2O sample (Figure 6c).

Under 1.33 kPa of ethanol during sample preparation and transportation to the KEK beamline (~12 h), a major part of Ag_2O was reduced to Ag^0 before UV−visible light irradiation based on the significantly reduced peak intensity for Ag−O interatomic pairs (Figure 6b-i, light on, 0 min). The weak peak became negligible within 10 min of UV−visible light irradiation, suggesting that most of the O sites (maximum 13.9 μmol) in Ag_2O were removed from Ag, whereas only 5.5 μmol of water was formed at 30 min of reaction, and the amount gradually increased until 4 h of reaction (32.1 μmol, Figure 1b-i). Thus, Ag_2O quickly reacted with C_2H_5OH, whereas CH_3CHO and H_2O desorption from the photocatalyst surface was slow. As the Ag−O peak disappeared, the peak due to the Ag−Ag interatomic pair gradually increased (Figure 6b-i), indicating that the Ag nanoparticle grew starting from the N value of 3.2 quickly to 8.3 and then converged to 10.1 (Figure 7i and Table 1i).

After the UV−visible light was turned off, the Ag−Ag peak became more intense because of the decrease of σ values within 10 min (Figures 6b-i and 7i, bottom), whereas the Ag−O peak recovered to the level before the UV−visible light irradiation. These facts suggested that the temperature decrease of Ag nanoparticles and the partial recovery of Ag_2O sites shifted from the dynamic charge equilibrium of the excited electron supply from the TiO_2 CB to Ag nanoparticles under UV−visible light and the oxidation effect probably by the O atoms at the interface between Ag and TiO_2.

Under 1.33 kPa of C_2H_5OH and 2.67 kPa of O_2, Ag sites in the initial Ag (2.0 wt %)−TiO_2 sample were more reduced before the UV−visible light irradiation based on the relatively weaker Ag−O peak and stronger Ag−Ag peak intensities compared with the data under ethanol only (Figure 6b-i and ii). However, under UV−visible light irradiation, the behavior of the Ag sites was very similar to that under the conditions of 1.33 kPa ethanol only (Figure 6b-i). Ethanol is an effective reducing agent for Ag sites; however, it may adsorb more strongly on the surface, whereas the hydrogen would combine with Ag_2O sites more quickly in the presence of an appropriate amount of O_2 by forming H_2O as suggested by the quicker H_2O formation under C_2H_5OH and O_2 versus that under C_2H_5OH (Figure 1b-i and ii). The N value for the Ag−Ag interatomic pair increased from 3.2 to 5.9 and then converged to 9.6 (Figure 7ii and Table 1ii) in a similar N value range to that under ethanol only (Figure 7i), whereas the σ values were, in general, smaller than those under ethanol only (Figure 7ii, bottom).

In contrast, under 1.33 kPa of C_2H_5OH and 5.32 kPa of O_2 (Figure 6b-iii), a relatively larger portion of Ag_2O sites versus Ag^0 sites remained before and after the UV−visible light irradiation (Figure 6b-iii) by the effect of the extra O_2 gas. The N value for the Ag−Ag interatomic pair increased from 2.5 to 5.5 and then converged to 8.6 (Figure 7iii and Table 1iii), significantly smaller than values under C_2H_5OH or under C_2H_5OH and O_2 (1:2 ratio) (Table 1i and ii. Thus, in the presence of 5.32 kPa of O_2 and UV−visible light irradiation, Ag^0 nanoparticles were smaller as a core and wrapped with a very thin Ag_2O shell.

Under the conditions of 1.33 kPa of ethanol, 2.67 kPa of O_2, and visible light irradiation (λ > 390 nm) as a control test, the Ag−O interatomic peak was weak/negligible, similar to the monitoring under UV−visible light (Figure 6b-ii and ii′); however, the Ag−Ag interatomic peak intensity did not increase much (Figure 6b-ii′) in comparison to the monitoring under UV−visible light (Figure 6b-ii). Conversely, after the UV−visible light was turned off, a quick increase of the peak was clearly observed within 20 min similar to all the other results depicted in Figure 6b-ii′. When the irradiation was visible light only (λ > 390 nm), the light negligibly activated TiO_2, and the electron flow from the TiO_2 CB to the Ag species was very limited and the growth of Ag^0 nanoparticles was significantly slower than that irradiated under UV−visible light.

Under these conditions, the N value increased starting from 3.2 to 6.6 and then converged to 8.7 (Figure 7ii′, top), smaller than the corresponding value of 9.6 under C_2H_5OH (1.33 kPa) and O_2 (5.32 kPa) under UV−visible light (Figure 7iii, top and Table 1ii and ii′). The reason the σ values were larger after the light was turned off than that before the irradiation (Figure 7ii′, bottom) was due to the structural disorder factor as discussed below.

Finally, on the basis of the curve-fit analysis, under the conditions of 1.33 kPa of ethanol, 2.67 kPa of O_2, and UV and IR light irradiation (245 nm < λ < 386 nm, λ > 686 nm), the Ag−Ag peak intensity gradually increased, greater than that under visible light but smaller than that under UV−visible light (Figure 6b-ii, ii′, and ii″). This fact suggested that the electron transfer from the CB of TiO_2 to Ag has a greater effect than LSPR of Ag for the Ag nanoparticle growth. In clear contrast to the other experiments using Ag (2.0 wt %)−TiO_2 (Figure 6b-i, ii, ii′, and iii), the Ag−Ag peak intensity negligibly changed when the UV−visible light was turned off (Figure 6b-ii′), suggesting that the UV and IR light did not heat Ag sites.

The σ value was calculated to be 0.009 95 nm for Ag metal at 290 K using the correlated Debye model[8,9,15] with the ab initio multiple-scattering calculation code, FEFF8.4,[42] and the Debye temperature of Ag bulk ($\theta_{D(\mathrm{bulk})}$ 225 K).[43] By the curve-fit analysis based on eq 5, the XDAP code[31] provides an experimental difference for the σ^2 value from that of the Ag metal (model). The initial σ value of 0.011 1 nm for Ag (2.0 wt %)−TiO_2 under C_2H_5OH (1.33 kPa) before UV−visible light irradiation quickly increased to 0.0123 nm (10 min of irradiation) and in turn slightly decreased to 0.011 9 nm (150 min of irradiation) as shown in Figure 7i. Then, the value quickly decreased to 0.0108 nm after the light was turned off at 170 min.

Furthermore, we evaluated the temperature at the Ag site based on the σ values. The temperature dependence of the σ value derived from FEFF8.4 combined with the correlated Debye model[8,9] for both bulk and surface Ag sites using the bulk and surface Debye temperature was previously reported.[15] We assumed that the thermodynamically stable face-centered cubic (fcc) (111) face had preferable exposure for the latter value ($\theta_{D(\mathrm{surf},\perp)}$ 155 K).[44,45] The Debye temperature for the lateral degree of freedom for Ag atoms at the fcc Ag(111) surface ($\theta_{D(\mathrm{surf},\parallel)}$) was 226 K,[45] very similar to the $\theta_{D(\mathrm{bulk})}$ (225 K). Therefore, we only considered the vertical degree of freedom at a free hemispherical surface of the Ag sphere corresponding to $\theta_{D(\mathrm{surf},\perp)}$, whereas two lateral degrees of freedom were considered to correspond to $\theta_{D(\mathrm{bulk})}$ if the Ag nanocrystals were sufficiently larger than a few nanometers. We also approximated the mean Ag nanoparticle temperature as the arithmetic mean temperature based on the $\theta_{D(\mathrm{surf},\perp)}$ weighted by $1/2{\cdot}1/3D$ [D: dispersion of nanoparticle (Table 1), for an effective vertical degree of freedom at a free hemispherical surface] and that based on the $\theta_{D(\mathrm{bulk})}$ weighted by $(1 - D) + 1/2D + 1/2{\cdot}2/3D$ for the bulk site, nonfree hemisphere in contact

https://doi.org/10.1021/acs.jpcc.1c04076
J. Phys. Chem. C 2021, 125, 14689−14701

Table 2. Coordination Number (N) and Debye−Waller Factor (σ) of the Ag−Ag Interatomic Pair Obtained for EXAFS of Ag (2.0 wt %)−TiO_2 (140 mg) (A) under C_2H_5OH (2.3 kPa) at the Controlled Temperatures at the Beamline versus (B) under Various Photocatalytic Conditions for 160−200 min and then in the Dark for 40−100 min (Figure 7)

		particle size and dispersion			correlated Debye model					
entry	T_{obs} (K)[a]	N[b]	$\bar{d}$ (nm)[c]	D[d]	σ (nm)[b]	$\sigma_{correlated\_Debye}$ (nm)[e]	$T_{D(bulk)}$ (K)[e]	$T_{D(surf,\perp)}$ (K)[e]	n[f]	$\sigma_{disorder}$ (nm)[g]
					(A) Thermally Grown					
i	301	4.9	0.97	0.99	0.011 3		377.7	176.7	2.31	0
ii	301	5.7	1.1	0.91	0.010 8		343.2	159.8	1.52	0
iii	343	7.1	1.4	0.77	0.011 2		372.5	174.1	1.16	0
iv	373	8.4	2.0	0.63	0.011 2	0.011 5	395.2	185.0	1	0
v	403	10.4	3.9	0.33	0.012 4	0.011 8	415.0	194.2	1	0.003 6
vi	343	10.3	3.8	0.34	0.011 1	0.010 9	353.8	165.2	1	0.001 8
vii	301	11.0	4.5	0.24	0.010 6	0.010 2	307.6	142.2	1	0.002 6
					(B) Light-Induced Grown					
i	300	10.1	3.6	0.38	0.010 7	0.010 3	310.6	143.6	1	0.002 9
ii	300	9.6	3.1	0.45	0.010 6	0.010 3	312.6	144.6	1	0.002 5
iii	300	8.6	2.1	0.60	0.010 7	0.010 4	317.1	146.6	1	0.002 5
ii′	300	8.7	2.2	0.59	0.011 1	0.010 4	316.7	146.5	1	0.004 0
ii″	300	8.1	1.8	0.66	0.011 0	0.010 4	318.9	147.5	1	0.003 6

[a]Sample temperature (T_{obs}) during EXAFS measurements. [b]Obtained based on EXAFS. [c]Ag nanoparticle size ($\bar{d}$) estimated based on the N value and ref 46. [d]Dispersion (D) estimated based on the N value and ref 46. [e]σ value, bulk temperature ($T_{D(bulk)}$), and surface temperature (perpendicular degree of freedom, $T_{D(surf,\perp)}$) corresponding to T_{obs} based on the correlated Debye model. [f]Degree of freedom effectively similar to vertical motion among vertical and lateral motions for Ag atoms at Ag nanoparticle size. [g]Structural disorder factor ($\sigma_{disorder}$) calculated based on eq 10.

with TiO_2 and two lateral degrees of freedom at a free hemispherical surface.[15]

However, for small Ag nanoparticles of size less than 2 nm based on the N values,[46] the lateral motions cannot be regarded as similar to that in the bulk but rather similar to vertical motion toward the Ag particle surface. We introduced the value n as the degrees of freedom for the surface Ag atom. Thus, in general, we approximated the temperature by the arithmetic mean temperature based on the $\theta_{D(surf,\perp)}$ weighted by $(1/2{\cdot}n/3)D$ for degrees of freedom effectively similar to vertical motion among vertical surfaces and lateral motions at a free hemispherical surface ($1 \leq n < 3$) and that based on the $\theta_{D(bulk)}$ weighted by $(1 - D) + 1/2\ D + (1/2{\cdot}(3 - n)/3)D$ for the bulk site, nonfree hemisphere in contact with TiO_2 and the rest of the degrees of freedom at a free hemispherical surface.

$$T_{eval} = nD/6T_{D(surf,\perp)} + (1 - nD/6)T_{D(bulk)} \quad (9)$$

To evaluate the dependence of n values on the Ag nanoparticle size, several Ag K-edge EXAFS spectra were measured for Ag (2.0 wt %)−TiO_2 under C_2H_5OH (1.33 kPa) by heating from 301 to 403 K and then back to 301 K in the dark (Table 2A-i−vii), and for a mean Ag particle size of 0.97−2.0 nm, the n values' dependence was drawn (Figure 8). When the mean Ag particle size was greater than 2.0 nm [N(Ag−Ag) > 8.4], the n value was 1.

The temperature-controlled EXAFS data for Ag (2.0 wt %)−TiO_2 under C_2H_5OH (1.33 kPa) required consideration of the structural disorder factor ($\sigma_{disorder}$)[47] once the sample was heated at 403 K as in eq 10 owing to the increase of structural disorder for thermally grown Ag nanocrystals of mean size of 3.9−4.5 nm:

$$\sigma^2 = \sigma_{correlated\_Debye}{}^2 + \sigma_{disorder}{}^2 \quad (10)$$

Assuming $\sigma_{disorder}$ values of 0.0018−0.0036 nm for such samples (Table 2A-v−vii), $\sigma_{correlated\_Debye}$ values corresponded well to the experimental temperature based on the approximation of eq 9 (Table 2A-iv−vii). The increase of structural disorder for Ag nanoparticles under C_2H_5OH (1.33 kPa)

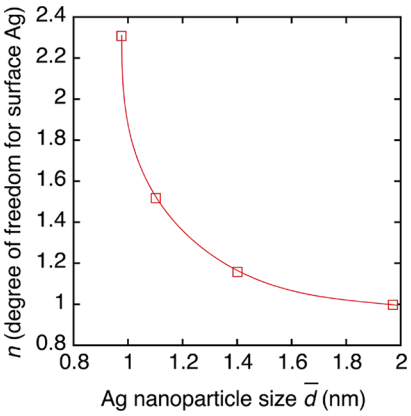

Figure 8. Adjustment of degrees of freedom for surface Ag atoms to correspond to the Debye temperature $\theta_{D(surf,\perp)}$ rather than $\theta_{D(bulk)}$ to evaluate the Ag site temperature based on eq 9 based on EXAFS measurements for Ag (2.0 wt %)−TiO_2 under C_2H_5OH at 301−373 K (Table 2).

suggested a relatively unsaturated metallic Ag surface under catalytic conditions.[48]

As a result, using Ag (2.0 wt %)−TiO_2 (0.100 g), C_2H_5OH (1.33 kPa), and UV−visible light, the initial temperature of 290 K before irradiation rose to 423 K after 10 min of irradiation and then reached an equilibrium temperature of ∼404 K after 50 min of light irradiation (Figure 7i, bottom). The initial CH_3CHO formation rate via eq 7 was 15.3 μmol h^{-1}, corresponding to an exothermic reaction at the rate of 2.17 J h^{-1} (Table 3i). On the basis of the molar heat capacity of Ag and TiO_2 ($C_{p,m}{}^{\circ}$ = 25.350 and 55.100 J K^{-1} mol^{-1}, respectively, 0.100 g of photocatalyst used),[49,50] the heat of reaction for CH_3CHO formation accounted for sample heating at a rate of 16 K per 30 min (Table 3i). This temperature accounts for the difference between the initial temperature peak at 10 min (423 K) and the equilibrium temperature (404 K) at 50−150 min of

https://doi.org/10.1021/acs.jpcc.1c04076
J. Phys. Chem. C 2021, 125, 14689−14701

Table 3. Heat of Reaction (Q) in the Initial 30 min of Reaction and Heat De-excited via LSPR under Photocatalytic Conditions of Ethanol Oxidation Using Ag (2.0 wt %)−TiO_2 (0.100 g)

	gas (kPa)							
ent.	ethanol	O_2	light	product	reaction	rate (μmol h^{-1})	T increase rate by Q (K min^{-1})	T increase rate by LSPR (K min^{-1})
i	1.33	0	full light	CH_3CHO	eq 7	15.3	0.54	49
ii		2.67		CH_3CHO	eq 1	64.2	11	
				CO_2	eq 2	51.3		
iii		5.32		CH_3CHO	eq 1	71.0	13	
				CO_2	eq 2	64.0		
ii′		2.67	$\lambda > 390$ nm	CH_3CHO	eq 7	18.6	0.65	
ii″			245 nm $< \lambda <$ 386 nm, $\lambda >$ 686 nm	CO_2	eq 2	9.4	1.5	0

photoreaction, the major energy source for heating Ag being light.

The Ag nanoparticles absorb light in the wavelength range 400−600 nm[17,28] (Figure 3) due to LSPR that de-excited to result in heat at a rate of 49 K min^{-1} (Table 3i). Thus, Ag nanoparticles were heated to the equilibrium temperature 404 K due to light energy and the heat dissipation to TiO_2 and then the glass reactor. The heat energy for CH_3CHO formation (eq 7) accounted for the initial extra temperature rise by 19 K compared with the equilibrium temperature of 404 K.

Under C_2H_5OH and O_2 with the molar ratio of 1:2, CH_3CHO and CO_2 were initially formed via eqs 1 and 2 at the rates of 64.2 and 51.3 μmol h^{-1}, respectively (Figure 1b-ii). The total heat of the reaction accounted for a temperature rise of 11 K min^{-1} (Table 3ii). The heat converted from Ag LSPR also heated the Ag nanoparticles at a rate of 49 K min^{-1} if all the light of wavelength 400−600 nm was absorbed. The temperature of the Ag nanoparticles soon reached equilibrium at ∼363 K within 10 min of reaction, significantly lower than those under ethanol only by 41 K (Figure 7i and ii, bottom). The formation of CH_3CHO and CO_2 stopped after 2 h of reaction because the reactants were totally consumed in the exothermic reactions of eqs 1, 2, and 8 (Figure 1b-ii).

In contrast, the equilibrium temperature remained constant at ∼363 K irrespective of the heat of reaction. Thus, the Ag site temperature rise and drop under light on and light off was mostly due to heat converted from Ag LSPR. A part of the heat derived from light energy and exothermic reaction was also used for Ag nanoparticle growth. The Ag sites were mostly the Ag^0 state during the EXAFS monitoring under UV−visible light (Figure 2b-ii); however, the LSPR peak intensity was weaker under C_2H_5OH and O_2 (1:2) compared with that under C_2H_5OH only (Figure 3c and d). Thus, surface O_2-derived species on Ag suppressed the light absorption by LSPR and lowered the equilibrated temperature due to the balance of mostly heat de-excited from LSPR and heat dissipation to ∼363 K (Figure 7ii, bottom).

Under C_2H_5OH and O_2 with the ratio of 1:4, initial CH_3CHO and CO_2 formation rates were 71.0 and 64.0 μmol h^{-1}, respectively, which accounted for a temperature rise of 13 K min^{-1} (Table 3iii). The temperature reached a maximum of 386 K at 20 min of reaction and equilibrated at ∼368 K. Similar to the monitoring under C_2H_5OH only and C_2H_5OH and O_2 (1:2), the temperature rise was mostly due to heat converted from Ag LSPR, but the initial maximum temperature was higher than equilibrium by 18 K due to the extra heat of reaction from faster CH_3CHO and CO_2 formation under C_2H_5OH and O_2 with the ratio of 1:4 (Figure 1b-iii). The similar equilibrium temperature, 368−363 K, under C_2H_5OH:O_2 = 1:2 was by the common effect of surface O_2-derived species on Ag reducing LSPR (Figure 3d and e).

It is implausible that surface O_2-derived species transferred over metallic Ag nanoparticles of 1.1−3.1 nm effectively block the irradiation of visible light of λ = 400−600 nm (Table 1ii and iii). Thus, surface O_2-derived species effectively suppressed the LSPR; the collective translational movement of surface Ag atoms and the light energy dissipated to TiO_2 and then the glass reactor resulting in lower equilibrium temperatures of 363−368 K in comparison to 404 K under ethanol only (Figure 7, bottom). Such a comparison was enabled by the local site temperature monitoring based on the correlated Debye model for the σ value of the local site in contrast to SERS monitoring, which requires a probe molecule;[18−20] phonon monitoring by Raman, which requires Si dots;[21] Raman spectroscopy, which requires locally doped ions;[22] and absorption spectroscopy, which requires laser irradiation.[23]

The Ag site temperature change under C_2H_5OH (1.33 kPa), O_2 (2.67 kPa), and visible light ($\lambda > 390$ nm) was interesting to compare with the other changes in view of the photocatalytic activation mechanism. Under the reaction conditions, O_2 activation over the TiO_2 surface was suppressed in the absence of UV light. The partial oxidation to CH_3CHO via eq 7 (Figure 1b-ii, right) accounted for the temperature increase of 0.65 K min^{-1}, whereas visible light led to a temperature increase of 49 K min^{-1} if all the light was absorbed (Table 3ii′). Thus, the temperature increase to 411 K after 20 min of reaction was due to major light energy via Ag LSPR. The equilibrated temperature was ∼406 K, similar to ∼404 K under ethanol and UV−visible light (Figure 7i and ii′, bottom). Thus, irradiated under visible light, O_2 was not activated over TiO_2, and surface O-free Ag nanoparticles were more effectively heated owing to LSPR. The broader Ag LSPR peak under the conditions suggested the difference of light absorption compared to that irradiated under UV−visible light (Figure 3d and f).

In clear contrast to all the other EXAFS monitoring (Figure 7i, ii, iii, and ii′), the Ag site temperature progressively increased under C_2H_5OH (1.33 kPa), O_2 (2.67 kPa), and UV and IR light (245 $< \lambda <$ 386 nm and $\lambda >$ 686 nm) (Figure 7ii″) by a self-acceleration mechanism due to the heat of reaction corresponding to a temperature increase of 1.5 K min^{-1} whereas there was no heat effect by light because LSPR did not occur in the absence of visible light irradiation (Table 3ii″). The catalyst heated by exothermic heat progressively increased the reaction rate.

In view of the accuracy of the site temperature evaluation based on the Debye−Waller factor, the method has been confirmed by tests on Ni, Mo, and Ag metal foils. The deviation between experiment and theory was already proved to be less than <8 K for the metal foils in the temperature range of 300−

https://doi.org/10.1021/acs.jpcc.1c04076
J. Phys. Chem. C 2021, 125, 14689−14701

400 K.[17] Our tentative study suggested that the Debye−Waller factor for Zr of ZrO_2 was negligibly changed by the UV−visible light irradiation[15−17] as well as that for Ti of TiO_2 in this study. As the Ag volume percent in Ag (2.0 wt %)−TiO_2 is only 0.80%, the heat exclusively transformed from LSPR at the Ag nanoparticle surface quickly dispersed to supporting TiO_2, and only a part of the light energy contributed to the dynamic temperature equilibrium at Ag (404−363 K).

This study extended the application to Ag nanoparticles growing from 0.50 to 3.6 nm in size under photocatalytic conditions (Table 1). By the introduction of an empirical n value for the degrees of freedom of surface Ag sites in eq 9 dependent on the Ag nanoparticle dispersion, the difference of the equilibrated temperature under light was demonstrated: 404−406 K under reductive conditions allowed partial oxidation in the absence of O_2 or the absence of O_2 activation (no UV light) (Figure 7i and ii′) versus 363−368 K under oxidative conditions to allow complete oxidation in the presence of both O_2 and UV light (Figure 7ii and iii).

The remaining difficulty in determining the temperature for growing Ag nanoparticles under photocatalytic conditions is the structural disorder factor (eq 10). The factor $\sigma_{disorder}$ was evaluated for a thermally heated Ag (2.0 wt %)−TiO_2 sample under C_2H_5OH at 403 K as reference tests: 0.0018−0.0036 nm (Table 2A-v−vii). The sample temperature after the UV and/or visible light was turned off in Figure 7 should converge soon to 300 K (ambient temperature inside the beamline after photocatalytic tests), whereas the evaluated temperature based on EXAFS was 326, 319, 317, 344, and 336 K (Figure 7). This is due to the increase of $\sigma_{disorder}$, and the value was evaluated to 0.0025−0.0040 nm due to the light-driven growth of Ag nanocrystals (Table 2B) in a similar range to 0.0018−0.0036 nm due to furnace heat-driven growth of Ag nanocrystals (Table 2A). This factor leads to a maximum 20 K overestimation for the Ag site temperature during light irradiation. Still, the effect of surface O species on Ag LSPR and accordingly heated temperature is certain in the comparison of the equilibrated temperature between 404−406 and 363−368 K. This method is expected to apply to real-time monitoring of catalysis that critically depends on the nanoparticle size, e.g., Au.[51]

CONCLUSIONS

In this paper, the reactivity and selectivity in C_2H_5OH photooxidation using Ag−TiO_2 photocatalysts were correlated to the temperature monitoring of Ag nanoparticles during the photocatalytic tests. On the basis of kinetic tests by varying the reactant ratio (C_2H_5OH:O_2) between 1:0 and 1:4, a major role of TiO_2 was the O_2 activation by UV light, whereas the Ag nanoparticle surface effectively allowed partial oxidation of C_2H_5OH to CH_3CHO and subsequent C−C bond cleavage to CO_2 and CH_4 by the combination of O species activated over TiO_2.

On the basis of the correlated Debye model for surface and bulk Ag sites in Ag nanoparticles, the Ag site temperature during the C_2H_5OH photooxidation reaction was monitored. In this paper, the temperature for Ag nanoparticles growing from 0.5 to 3.6 nm was successfully monitored on the basis of the evaluation of the effective degrees of freedom for translational motion of surface Ag sites as well as the correlated Debye model. The equilibrated temperature during photocatalysis was as high as 404−406 K to allow partial oxidation to CH_3CHO over the Ag^0 surface heated by the converted energy from Ag LSPR due to visible light when O_2 or UV light was absent. In contrast, the equilibrated temperature was 363−368 K under O_2 and UV light, lower by suppressed Ag LSPR by O_2-derived species activated on TiO_2 and transferred to Ag to allow complete oxidation to CO_2 and the other product due to C−C bond cleavage: CH_4. In oxidative conditions, O_2-derived species were not detected by EXAFS curve-fit analysis but could be monitored as the temperature decreased by 40 K to suppress Ag LSPR in accord with the LSPR peak intensity change under photocatalytic conditions.

ASSOCIATED CONTENT

Supporting Information

The Supporting Information is available free of charge at https://pubs.acs.org/doi/10.1021/acs.jpcc.1c04076.

Experimental details for photocatalytic tests and synchrotron X-ray measurements and the summary of EXAFS χ-function oscillations (PDF)

AUTHOR INFORMATION

Corresponding Author

Yasuo Izumi − *Department of Chemistry, Graduate School of Science, Chiba University, Chiba 263-8522, Japan;* orcid.org/0000-0001-8366-1864; Phone: +81-43-290-3696; Email: yizumi@faculty.chiba-u.jp; Fax: +81-43-290-2783

Authors

Daiki Fukuhara − *Department of Chemistry, Graduate School of Science, Chiba University, Chiba 263-8522, Japan*

Moses Tuhafeni Joseph − *Department of Chemistry, Graduate School of Science, Chiba University, Chiba 263-8522, Japan;* orcid.org/0000-0003-4663-1628

Tarik Loumissi − *Department of Chemistry, Graduate School of Science, Chiba University, Chiba 263-8522, Japan;* orcid.org/0000-0002-4840-8625

Chao Zhang − *Department of Chemistry, Graduate School of Science, Chiba University, Chiba 263-8522, Japan*

Takaomi Itoi − *Department of Mechanical Engineering, Graduate School of Engineering, Chiba University, Chiba 263-8522, Japan;* orcid.org/0000-0002-2864-6650

Hongwei Zhang − *Department of Chemistry, Graduate School of Science, Chiba University, Chiba 263-8522, Japan;* orcid.org/0000-0002-6773-8769

Complete contact information is available at: https://pubs.acs.org/10.1021/acs.jpcc.1c04076

Author Contributions

D.F., M.T.J., T.L., T.I., C.Z., and H.Z. wrote part of the manuscript. Y.I. supervised the research and wrote most of the manuscript.

Notes

The authors declare no competing financial interest.

ACKNOWLEDGMENTS

The authors are grateful for the financial support obtained from Grants-in-Aid for Scientific Research B (20H02834) and C (17K05961) from the Japan Society for the Promotion of Science. X-ray absorption experiments were performed with the approval of the Photon Factory Proposal Review Committee (2020G676, 2019G141, and 2018G649). The authors thank Enago (www.enago.jp) for the English language review.

REFERENCES

(1) Hoffmann, M. R.; Martin, S. T.; Choi, W.; Bahnemann, D. W. Environmental Applications of Semiconductor Photocatalysis. *Chem. Rev.* **1995**, *95*, 69−96.

(2) Martin, S. T.; Morrison, C. L.; Hoffmann, M. R. Photochemical Mechanism of Size-Quantized Vanadium-Doped TiO_2 Particles. *J. Phys. Chem.* **1994**, *98*, 13695−13704.

(3) Emeline, A. V.; Ryabchuk, V. K.; Serpone, N. Dogma and Misconceptions in Heterogenous Photocatalysis. Some Enlightened Reflections. *J. Phys. Chem. B* **2005**, *109*, 18515−18521.

(4) Izumi, Y. Recent Advances in Photocatalytic Conversion of Carbon Dioxide into Fuels with Water and/or Hydrogen Using Solar Energy and Beyond. *Coord. Chem. Rev.* **2013**, *257*, 171−186.

(5) Izumi, Y. Recent Advances (2012−21015) in the Photocatalytic Conversion of Carbon Dioxide to Fuels Using Solar Energy: Feasibility for a New Energy. In *Advances in CO_2 Capture, Sequestration, and Conversion*; Jin, F., He, L.-N., Hu, Y. H., Eds.; ACS Publishications: Washington, DC, 2015; Chapter 1, Vol. *1194*, pp 1−46.

(6) Chen, X.; Mao, S. S. Titanium Dioxide Nanomaterials: Synthesis, Properties, Modifications, and Applications. *Chem. Rev.* **2007**, *107*, 2891−2959.

(7) Naya, S.; Kimura, K.; Tada, H. One-Step Selective Aerobic Oxidation of Amines to Imines by Gold Nanoparticle-Loaded Rutile Titanium(IV) Oxide Plasmon Photocatalyst. *ACS Catal.* **2013**, *3*, 10−13.

(8) Beni, G.; Platzman, P. M. Temperature and Polarization Dependence of Extended X-Ray Absorption Fine-Structure Spectra. *Phys. Rev. B* **1976**, *14*, 1514−1518.

(9) Sevillano, E.; Meuth, H.; Rehr, J. J. Extended X-Ray Absorption Fine Structure Debye-Waller Factors. I. Monoatomic Crystals. *Phys. Rev. B: Condens. Matter Mater. Phys.* **1979**, *20*, 4908−4911.

(10) Clavero, C. Plasmon-Induced Hot-Electron Generation at Nanoparticle/Metal-Oxide Interfaces for Photovoltaic and Photocatalytic Devices. *Nat. Photonics* **2014**, *8*, 95−103.

(11) Nikawa, T.; Naya, S.; Tada, H. Rapid Removal and Decomposition of Gaseous Acetaldehyde by the Thermo- and Photocatalysis of Gold Nanoparticle-Loaded Anatase Titanium(IV) Oxide. *J. Colloid Interface Sci.* **2015**, *456*, 161−165.

(12) Zhang, Z.; Zhang, C.; Zheng, H.; Xu, H. Plasmon-Driven Catalysis on Molecules and Nanomaterials. *Acc. Chem. Res.* **2019**, *52*, 2506−2515.

(13) Cushing, S. K.; Li, J.; Meng, F.; Senty, T. R.; Suri, S.; Zhi, M.; Li, M.; Bristow, A. D.; Wu, N. Photocatalytic Activity Enhanced by Plasmonic Resonant Energy Transfer from Metal to Semiconductor. *J. Am. Chem. Soc.* **2012**, *134*, 15033−15041.

(14) Furube, A.; Du, L.; Hara, K.; Katoh, R.; Tachiya, M. Ultrafast Plasmon-Induced Electron Transfer from Gold Nanodots into TiO_2 Nanoparticles. *J. Am. Chem. Soc.* **2007**, *129*, 14852−14853.

(15) Zhang, H.; Itoi, T.; Konishi, T.; Izumi, Y. Dual Photocatalytic Roles of Light: Charge Separation at the Band Gap and Heat via Localized Surface Plasmon Resonance To Convert CO_2 into CO over Silver-Zirconium Oxide. *J. Am. Chem. Soc.* **2019**, *141*, 6292−6301.

(16) Zhang, H.; Itoi, T.; Niki, K.; Konishi, T.; Izumi, Y. Dual Origins of Photocatalysis: Light-Induced Band-Gap Excitation of Zirconium Oxide and Ambient Heat Activation of Gold to Enable $^{13}CO_2$ Photoreduction/Conversion. *Catal. Today* **2020**, *356*, 544−556.

(17) Zhang, H.; Itoi, T.; Konishi, T.; Izumi, Y. Efficient and Selective Interplay Revealed: CO_2 Reduction to CO over ZrO_2 by Light with Further Reduction to Methane over Ni^0 by Heat Converted from Light. *Angew. Chem., Int. Ed.* **2021**, *60*, 9045−9054.

(18) Yang, H.; He, L.; Hu, Y.; Lu, X.; Li, G.; Liu, B.; Ren, B.; Tong, Y.; Fang, P. Quantitative Detection of Photothermal and Photoelectrocatalytic Effects Induced by SPR from Au@Pt Nanoparticles. *Angew. Chem., Int. Ed.* **2015**, *54*, 11462−11466.

(19) Liu, L.; Li, D.; Deng, W. Stimuli-Responsive Microgels with Fluorescent and SERS Activities for Water and Temperature Sensing. *Biosens. Bioelectron.* **2021**, *180*, 113138.

(20) Mao, C.; Li, H.; Gu, H.; Wang, J.; Zou, Y.; Qi, G.; Xu, J.; Deng, F.; Shen, W.; Li, J.; et al. Beyond the Thermal Equilibrium Limit of Ammonia Synthesis with Dual Temperature Zone Catalyst Powered by Solar Light. *Chem.* **2019**, *5*, 2702−2717.

(21) Agarwal, D.; Aspetti, C. O.; Cargnello, M.; Ren, M.; Yoo, J.; Murray, C. B.; Agarwal, R. Engineering Localized Surface Plasmon Interactions in Gold by Silicon Nanowire for Enhanced Heating and Photocatalysis. *Nano Lett.* **2017**, *17*, 1839−1845.

(22) Hartman, T.; Geitenbeek, R. G.; Wondergem, C. S.; van der Stam, W.; Weckhuysen, B. M. Operando Nanoscale Sensors in Catalysis: All Eyes on Catalyst Particles. *ACS Nano* **2020**, *14*, 3725−3735.

(23) Yen, C.-W.; El-Sayed, M. A. Plasmonic Field Effect on the Hexacyanoferrate (III)-Thiosulfate Electron Transfer Catalytic Reaction on Gold Nanoparticles: Electromagnetic or Thermal? *J. Phys. Chem. C* **2009**, *113*, 19585−19590.

(24) Urushidate, K.; Hara, K.; Yoshiba, M.; Kojima, T.; Itoi, T.; Izumi, Y. Optimization of High Voltage-Type Solar Cell Comprising Thin TiO_2 on Anode and Thin Ag-TiO_2 Photocatalysts on Cathode. *Sol. Energy* **2020**, *208*, 604−611.

(25) Ogura, Y.; Okamoto, S.; Itoi, T.; Fujishima, Y.; Yoshida, Y.; Izumi, Y. A Photofuel Cell Comprising Titanium Oxide and Silver(I/0) Photocatalysts for Use of Acidic Water as a Fuel. *Chem. Commun.* **2014**, *50*, 3067−3070.

(26) Ahmed, N.; Shibata, Y.; Taniguchi, T.; Izumi, Y. Photocatalytic Conversion of Carbon Dioxide into Methanol Using Zinc-Copper-M(III) (M = Aluminum, Gallium) Layered Double Hydroxides. *J. Catal.* **2011**, *279*, 123−135.

(27) Masih, D.; Yoshitake, H.; Izumi, Y. Photo-oxidation of Ethanol on Mesoporous Vanadium-Titanium Oxide Catalysts and the Relation to Vanadium(IV) and (V) Sites. *Appl. Catal., A* **2007**, *325*, 276−282.

(28) Yoshida, Y.; Itoi, T.; Izumi, Y. Preferential Photooxidation of CO in Hydrogen across the Crystalline Face Boundary over Spheroidal ZnO Promoted by Cu Ions. *J. Phys. Chem. C* **2015**, *119*, 21585−21598.

(29) Transmittance of light as a function of wavelength. https://www.hoyacandeo.co.jp/japanese/products/eo/color/10.html (accessed June 14, 2021).

(30) Bearden, J. A. X-Ray Wavelengths. *Rev. Mod. Phys.* **1967**, *39*, 78−124.

(31) Vaarkamp, M.; Linders, H.; Koningsberger, D. *XDAP*, Version 2.2.7; XAFS Services International: Woudenberg, The Netherlands, 2006.

(32) Liu, L. G.; Bassett, W. A. Compression of Ag and Phase Transformation of NaCl. *J. Appl. Phys.* **1973**, *44*, 1475−1479.

(33) Petitjean, C.; Horwat, D.; Pierson, J. F. Structure-Properties Relationship in Reactively Sputtered Ag-Cu-O Films. *J. Phys. D: Appl. Phys.* **2009**, *42*, 025304.

(34) Nadeem, M. A.; Idriss, H. Effect of Temperature on the Photoreactions of Ethanol over Ag/TiO_2 in Steady State Catalytic Conditions. *Appl. Catal., B* **2021**, *284*, 119736.

(35) Menési, J.; Kékesi, R.; Körösi, L.; Zöllmer, V.; Richardt, A.; Dékány, I. The Effect of Transition Metal Doping on the Photooxidation Process of Titania-Clay Composites. *Int. J. Photoenergy* **2008**, *2008*, 846304.

(36) Veres, Á.; Menési, J.; Juhász, Á.; Berkesi, O.; Ábrahám, N.; Bohus, G.; Oszkó, A.; Pótári, G.; Buzás, N.; Janovák, L.; et al. Photocatalytic Performance of Silver-Modified TiO_2 Embedded in Poly(Ethyl-Acrylate-Co-Methyl Metacrylate) Matrix. *Colloid Polym. Sci.* **2014**, *292*, 207−217.

(37) Tallósy, S. P.; Janovák, L.; Nagy, E.; Deák, Á.; Juhász, Á.; Csapó, E.; Buzás, N.; Dékány, I. Adhesion and Inactivation of Gram-Negative and Gram-Positive Bacteria on Photoreactive TiO_2/Polymer and Ag-TiO_2/Polymer Nanohybrid Films. *Appl. Surf. Sci.* **2016**, *371*, 139−150.

(38) Kawamura, S.; Puscasu, M. C.; Yoshida, Y.; Izumi, Y.; Carja, G. Tailoring Assemblies of Plasmomic Silver/Gold and Zinc-Gallium Layered Double Hydroxides for Photocatalytic Conversion of Carbon Dioxide Using UV-Visible Light. *Appl. Catal., A* **2015**, *504*, 238−247.

(39) Urushidate, K.; Li, J.; Hara, K.; Kojima, T.; Izumi, Y. Polarizability and Catalytic Activity Determine Good Titanium Oxide Crystals but Not Homogeneity in Solar Cells Using Photocatalysts on Both Electrodes. *ACS Sustainable Chem. Eng.* **2020**, *8*, 1406−1416.

https://doi.org/10.1021/acs.jpcc.1c04076
J. Phys. Chem. C 2021, 125, 14689−14701

(40) Du, P.; Cao, Y.; Liu, Z.; Kong, X.; Sun, Z.; Li, D. Synthesis of Thermally Stable Ag@TiO_2 Core-Shell Nanoprisms and Plasmon-Enhanced Optical Properties for a P3HT Thin Film. *RSC Adv.* **2013**, *3*, 6016−6021.
(41) Hyde, B. G.; Andersson, S. *Inorganic Crystal Structures*; John Wiley & Sons: New York, 1989.
(42) Ankudinov, L.; Ravel, B.; Rehr, J. J.; Conradson, S. D. Real-Space Multiple-Scattering Calculation and Interpretation of X-Ray-Absorption Near-Edge Structure. *Phys. Rev. B: Condens. Matter Mater. Phys.* **1998**, *58*, 7565−7576.
(43) *American Institute of Physics Handbook*, third ed.; Gray, D. E., Ed.; McGraw-Hill: New York, 1972; p 4-116.
(44) Morabito, J. B., Jr.; Steiger, R. F.; Somorjai, G. A. Studies of the Mean Displacement of Surface Atoms in the (1 0 1) and (1 1 0) Faces of Silver Single Crystals at Low Temperatures. *Phys. Rev.* **1969**, *179*, 638−644.
(45) *Springer Handbook of Condensed Matter and Materials Data*; Martienssen, W., Warlimont, H., Eds.; Springer: Heidelberg, Germany, 2005; p 1013.
(46) Kip, B. J.; Duivenvoorden, F. B. M.; Koningsberger, D. C.; Prins, R. Determination of Metal Particle Size of Highly Dispersed Rh, Ir, and Pt Catalysts by Hydrogen Chemisorption and EXAFS. *J. Catal.* **1987**, *105*, 26−38.
(47) Sayers, D. E.; Bunker, B. A. Data Analysis. In *X-Ray Absorption-Principles, Applications, Techniques of EXAFS, SEXAFS, and XANES*; Koningsberger, D. C., Prins, R., Eds.; Wiley: New York, 1988; p 245.
(48) Matsubara, K.; Kelly, K. L.; Sakai, N.; Tatsuma, T. Plasmon Resonance-Based Photoelectrochemical Tailoring of Spectrum, Morphology, and Orientation of Ag Nanoparticles on TiO_2 Single Crystals. *J. Mater. Chem.* **2009**, *19*, 5526−5532.
(49) *CRC Handbook of Chemistry and Physics*, 96th ed,; Haynes, W. M., Ed.; CRC Press: Boca Raton, FL, 2015; p 4-124.
(50) Smith, S. J.; Stevens, R.; Liu, S.; Li, G.; Navrotsky, A.; Boerio-Goates, J.; Woodfield, B. F. Heat Capacities and Thermodynamic Functions of TiO_2 Anatase and Rutile: Analysis of Phase Stability. *Am. Mineral.* **2009**, *94*, 236−243.
(51) Bell, A. T. The Impact of Nanoscience on Heterogeneous Catalysis. *Science* **2003**, *299*, 1688−1691.

https://doi.org/10.1021/acs.jpcc.1c04076
J. Phys. Chem. C 2021, 125, 14689−14701